Available online at www.sciencedirect.com
ScienceDirect
Journal of Magnetic Resonance 183 (2006) 252–258
JMR Journal of Magnetic Resonance
www.elsevier.com/locate/jmr

Double-quantum filtered rotational-echo double resonance ☆

Shigeru Matsuoka, Jacob Schaefer *

Department of Chemistry, Washington University, St. Louis, MO 63130, USA

Received 19 June 2006; revised 14 August 2006
Available online 27 September 2006

Abstract

The homonuclear scalar coupling of a directly bonded ^{13}C–^{13}C pair has been used to create a double-quantum filter (DQF) to remove the natural-abundance ^{13}C background in $^{13}C\{^{15}N\}$ rotational-echo double-resonance (REDOR) experiments. The DQF scalar and REDOR dipolar evolution periods are coincident which is important for sensitivity in the event of weak ^{13}C–^{15}N dipolar coupling. Calculated and observed $^{13}C\{^{15}N\}$ DQF–REDOR dephasings were in agreement for a test sample of mixed recrystallized labeled alanines. Glycine metabolism in a single *uniform*-^{15}N soybean leaf labeled for 6 min by $^{13}CO_2$ was measured quantitatively by $^{13}C\{^{15}N\}$ DQF–REDOR with no background interferences.

Keywords: Dipolar coupling; Glycine metabolism; Magic-angle spinning; Photorespiration; Photosynthesis; Solid-state NMR; Soybean leaves

1. Introduction

Rotational-echo double resonance (REDOR)[1] [1] has been widely used over the last 15 years to measure internuclear distances quantitatively in isolated (*I*–*S*) spin pairs [2]. These pairs are generally introduced by specific stable-isotope labeling. In many practical applications of REDOR, the signal from the label is small compared to the signal from the natural-abundance background. This complicates the determination of the REDOR full-echo signal (S_0) and therefore the scaling [3] of the REDOR difference signal ($\Delta S = S_0 - S$), where S is the signal observed with *I*-spin dephasing pulses.

A strategy to deal with this complication has been the use of a third hetero label as a helper [4]. For example, the specific labeling of A_{10} and G_{11} by L-[1-^{13}C]alanine and [^{15}N]glycine, respectively, in a 21-residue synthetic analogue of the peptide antibiotic, magainin, resulted in a double-labeled peptide bond in the middle of the 21-mer [5]. A cross-polarization transfer from protons to nitrogens for this peptide in a lipid bilayer, followed by an $^{15}N \rightarrow {}^{13}C$ coherence transfer (TEDOR) [6], produced a full-echo signal that arose from just the ^{13}C labels in A_{10}. A subsequent $^{13}C\{^{19}F\}$ REDOR dephasing period produced dephasing arising from proximity to a second magainin analogue (specifically labeled by L-[3-^{19}F]alanine at A_{10}) that had also been inserted in the bilayer. Detailed analysis of the dephasing was interpreted in terms of the formation of peptide aggregates [5].

A limitation on the popularity of a helper spin in so-called TEDOR–REDOR [7] and double-REDOR [8] experiments of the type described above is the need for a probe capable of accepting high-power pulses at four different radiofrequencies [9]. In this report, we describe an alternate strategy that may be useful in some applications. If a site can be *I*-spin double-labeled in such a way that there is a significant *I*-spin homonuclear coupling (as in ^{13}C–^{13}C

☆ This paper is based on work supported by the Naito Foundation of Japan and by the National Science Foundation (under Grant No. MCB-0089905).
* Corresponding author. Fax: +1 314 935 4481.
E-mail address: jschaefer@wustl.edu (J. Schaefer).
[1] *Abbreviations used:* CPMAS, cross-polarization magic-angle spinning; DQF, double-quantum filter; INADEQUATE, incredible natural-abundance double-quantum transfer experiment; REDOR, rotational-echo double resonance; TEDOR, transferred-echo double resonance.

1090-7807/$ - see front matter © 2006 Elsevier Inc. All rights reserved.
doi:10.1016/j.jmr.2006.08.010

directly bonded pairs, for example), then dipolar coupling to a second *S*-spin label can be measured with no interference from the natural-abundance background. A homonuclear double-quantum filter (DQF) [10] provides the required selectivity rather than a third hetero label.

Double-quantum filtering (excitation and reconversion) using strong ^{13}C–^{13}C dipolar coupling followed by weak REDOR dephasing is not an option because of interferring dephasing by ^{13}C–^{13}C scalar *J* coupling during the long REDOR evolution period. Instead, the homonuclear *J* coupling is itself used for filtering *during* the REDOR evolution. A *J*-based ^{13}C–^{13}C double-quantum filter (INADEQUATE) [11] has been developed for solution-state NMR. INADEQUATE results in anti-phase line shapes which are not a problem for well-resolved peaks but cause self-cancellation of broader signals. A refocused version of INADEQUATE [12–14] that avoids anti-phase line shapes is therefore better suited to solid-state NMR and DQF–REDOR.

2. Experiments

Spectra were obtained of the mix of labeled and unlabeled alanines shown in Fig. 1 using a 6-frequency transmission-line probe [15], having a 12-mm long, 6-mm inside-diameter analytical coil and a Chemagnetics/Varian magic-angle spinning ceramic stator. Lyophilized samples were contained in thin-wall Chemagnetics/Varian 5-mm outside-diameter zirconia rotors. The rotor speed was under active control to within ±2 Hz. The spectrometer was controlled by a Tecmag Libra pulse programmer. Radiofrequency pulses for ^{13}C (125 MHz) and ^{15}N (50.3 MHz) were produced by 2-kW American Microwave Technology power amplifiers. Proton (500 MHz) radiofrequency pulses were generated by a 2-kW Amplifier Systems tube amplifiers driven by a 50-W American Microwave Technology power amplifier. The π-pulse lengths were 8 μs for ^{13}C and 9 μs for ^{15}N. The amplitudes of all pulses were under active control [16]. REDOR dephasing pulses followed the xy8 phase-cycling scheme [17]. A 12-T static magnetic field was provided by an 89-mm bore Magnex superconducting solenoid. Proton–carbon cross-polarization magic-angle spinning transfers were made with radiofrequency fields of 62.5 kHz. Proton dipolar decoupling was 100 kHz during data acquisition. TPPM modulation [18] of the proton radiofrequency was generated by an external device running asynchronously with respect to the pulse-programmer clock. REDOR spectra were acquired on an alternate-scan basis, first S then S_0.

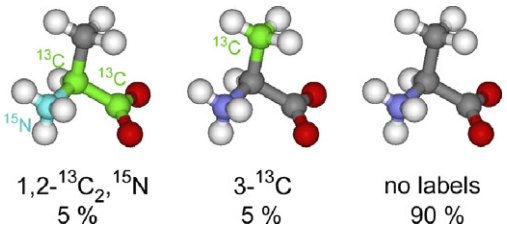

Fig. 1. Composition of a mixture of two labeled L-alanines with natural-abundance L-alanine, $^{+}NH_3CH(-CH_3)C(=O)O^{-}$. The three alanines were recrystallized together from water.

3. Results and discussion

3.1. Interleaving double-quantum filtering and REDOR

We used the high-efficiency *J*-based double-quantum filter pulse sequence (Fig. 2 and Table 1) introduced for solids by Mueller et al. [14]. REDOR *S*-spin pulses ($I = {}^{13}C$, $S = {}^{15}N$) created dephasing during the two τ–π–τ periods of the sequence. A single ^{15}N π/2 pulse was inserted between the ^{13}C ϕ_3 and ϕ_4 pulses for both full-echo (without ^{15}N π pulses) and dephased-echo (with ^{15}N π pulses) REDOR acquisitions. The ^{15}N π/2 pulse ensured that bilinear coherence generated during the first τ–π–τ dephasing period was not refocused as observable single-quantum coherence during the second period (Fig. 3). As a result, double-quantum filtering and REDOR dephasing could

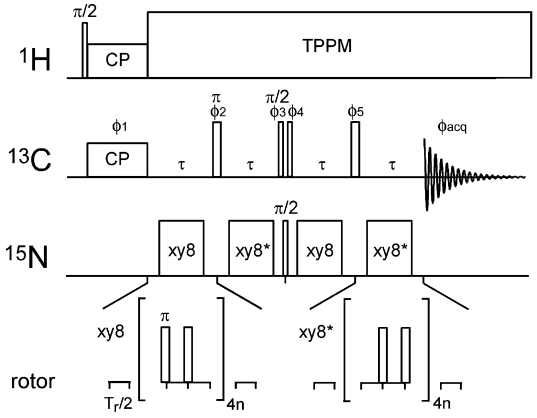

Fig. 2. Pulse sequence for double-quantum filtered (DQF) $^{13}C\{^{15}N\}$ rotational-echo double resonance (REDOR). The DQF scheme is that of Mueller et al. [14]. The ^{15}N π/2 pulse is used to acquire both full-echo (S_0) and dephased (S) signals. The ^{15}N π pulses are used only to acquire S, and their phases follow the xy8 scheme of Gullion et al. [17]. Phases of the ^{13}C pulses are listed in Table 1.

Table 1
Phase cycling for the DQF–REDOR sequence of Fig. 2

Pulse	Phase
^{1}H π/2	$(X \times 8, \overline{X} \times 8) \times 2$
^{1}H CP	$Y \times 32$
ϕ_1 (^{13}C CP)	$X \times 16, \overline{Y} \times 16$
ϕ_2 (^{13}C π)	$X \times 16, Y \times 16$
ϕ_3 (^{13}C π/2)	$Y \times 16, X \times 16$
ϕ_4 (^{13}C π/2)	$(Y, X, \overline{Y}, \overline{X}) \times 4, (\overline{Y}, \overline{X}, Y, X) \times 4$
ϕ_5 (^{13}C π)	$(X, Y, \overline{X}, \overline{Y}, \overline{X}, \overline{Y}, X, Y, Y, \overline{X}, \overline{Y}, X, \overline{Y}, X, Y, \overline{X}) \times 2$
ϕ_{acq}	$(X, Y, \overline{X}, \overline{Y}) \times 8$

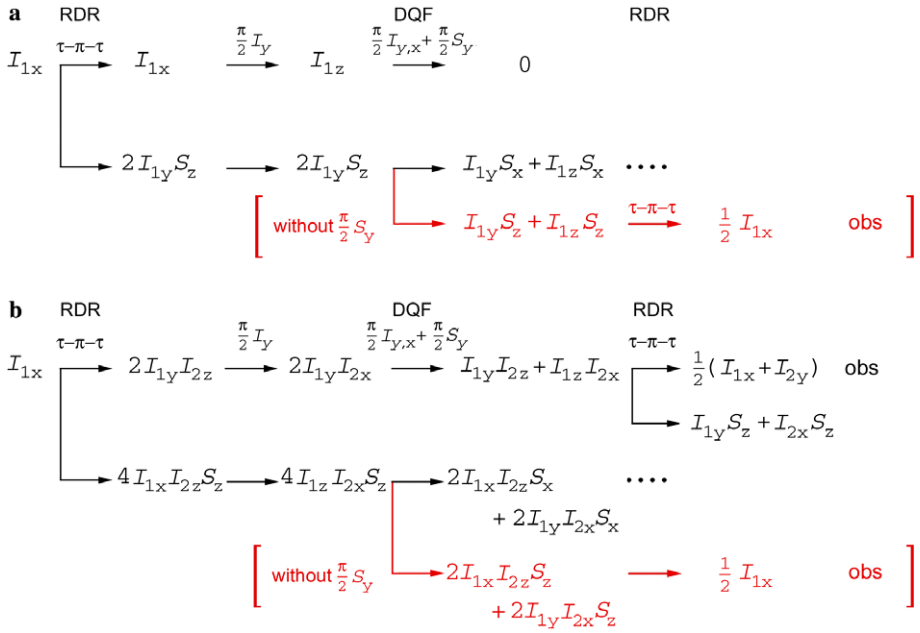

Fig. 3. Observable single-quantum coherence, non-observable double-quantum coherence, and non-observable bi- and tri-linear coherences using the pulse sequence of Fig. 2 for (a) a ^{13}C–^{15}N spin pair and (b) a ^{13}C–^{13}C–^{15}N spin system ($I = {}^{13}C$, $S = {}^{15}N$). The illustration is the average from the first two phase entries of Table 1. The full double-quantum filter is the average from the first four entries.

be done simultaneously rather than sequentially, an important feature in the event of weak heteronuclear coupling.

3.2. Theoretical description of DQF–REDOR

Using an independent coordinate system for directly bonded I-spins 1 and 2 (Fig. 4, left), we define dipolar couplings to a single S spin and the accumulated REDOR phases by [1,14]

$$D_{(1)}(r_1) = \gamma_I\gamma_S h/2\pi r_1^3 \tag{1}$$

$$D_{(2)}(r_2) = \gamma_I\gamma_S h/2\pi r_2^3 \tag{2}$$

$$\omega_{D(1)}(r_1,\alpha_1,\beta_1;t) = \pm\tfrac{1}{2}D_{(1)}(r_1)[\sin^2\beta_1\cos 2(\alpha_1+\omega_r t) - \sqrt{2}\sin 2\beta_1\cos(\alpha_1+\omega_r t)] \tag{3}$$

$$\begin{aligned}\overline{\omega}_{D(1)}(r_1,\alpha_1,\beta_1) &= \pm\frac{1}{T_r}\left[\int_0^{T_r/2}\omega_{D(1)}(r_1,\alpha_1,\beta_1;t)\,dt - \int_{T_r/2}^{T_r}\omega_{D(1)}(r_1,\alpha_1,\beta_1;t)\,dt\right]\\ &= \pm\frac{D_{(1)}(r_1)}{4\pi}\{\sin^2\beta_1[\sin 2(\alpha_1+\pi)-\sin 2\alpha_1] - 2\sqrt{2}\sin 2\beta_1[\sin(\alpha_1+\pi)-\sin\alpha_1]\}\\ &= \pm\frac{\sqrt{2}D_{(1)}(r_1)}{\pi}\sin 2\beta_1\sin\alpha_1\end{aligned} \tag{4}$$

$$\Delta\Phi_{(1)}(r_1,\alpha_1,\beta_1) = \overline{\omega}_{D(1)}(r_1,\alpha_1,\beta_1)N_cT_r \tag{5}$$

$$\overline{\omega}_{D(2)}(r_2,\alpha_2,\beta_2) = \pm\frac{\sqrt{2}D_{(2)}(r_2)}{\pi}\sin 2\beta_2\sin\alpha_2 \tag{6}$$

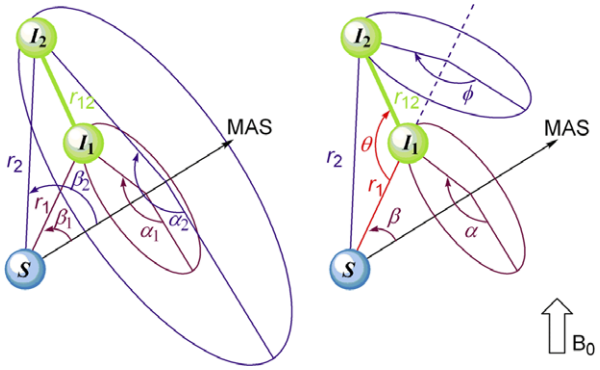

Fig. 4. Two coordinate systems for an I_2S spin system.

$$\Delta\Phi_{(2)}(r_2,\alpha_2,\beta_2) = \overline{\omega}_{D(2)}(r_2,\alpha_2,\beta_2)N_cT_r \tag{7}$$

The distribution of angles (α_2,β_2) is connected to that of angles (α_1,β_1) by the ^{15}N–^{13}C–^{13}C angle and ^{13}C–^{13}C (r_{12}) distance. A correlated coordinate system (Fig. 4, right) is therefore necessary for general numerical calculations of DQF–REDOR. In this coordinate system,

$$r_2(r_1,\theta) = \sqrt{r_1^2 + r_{12}^2 - 2r_1r_{12}\cos\theta} \tag{8}$$

$$D_{(2)}(r_1,\theta) = \gamma_I\gamma_S h/2\pi r_2(r_1,\theta)^3 \tag{9}$$

$$\overline{\omega}_{D(1)}(r_1,\alpha_1,\beta_1) \equiv \overline{\omega}_{D(1)}(r_1,\alpha,\beta) \tag{10}$$

$$\Delta\Phi_{(1)}(r_1,\alpha,\beta) = \overline{\omega}_{D(1)}(r_1,\alpha,\beta)N_cT_r \tag{11}$$

$$\overline{\omega}_{D(2)}(r_2,\alpha_2,\beta_2) \equiv \overline{\omega}_{D(2)}(r_1,\alpha,\beta,\phi,\theta) \tag{12}$$

$$\Delta\Phi_{(2)}(r_1,\alpha,\beta,\phi,\theta) = \overline{\omega}_{D(2)}(r_1,\alpha,\beta,\phi,\theta)N_cT_r \tag{13}$$

Signal modulation of the observable magnetization $I\{S\}$ DQF–REDOR (see Fig. 3b) by D_{IS}, J_{II} and T'_2 relaxation is given by [14]

$$I_{1x} \xrightarrow{\text{RDR}} 2I_{1y}I_{2z}\cos(\Delta\Phi_{(1)})\sin(2\pi J_{II}\tau)\exp\left(\frac{-2\tau}{T'_{2(1)}}\right) \tag{14}$$

$$\xrightarrow{\text{DQF}} I_{1y}I_{2z}\cos(\Delta\Phi_{(1)})\sin(2\pi J_{II}\tau)\exp\left(\frac{-2\tau}{T'_{2(1)}}\right) + I_{1z}I_{2x}\cos(\Delta\Phi_{(1)})\sin(2\pi J_{II}\tau) \times \exp\left(\frac{-2\tau}{T'_{2(1)}}\right) \tag{15}$$

$$\xrightarrow{\text{RDR}} \frac{1}{2}I_{1x}\cos^2(\Delta\Phi_{(1)})\sin^2(2\pi J_{II}\tau)\exp\left(\frac{-4\tau}{T'_{2(1)}}\right) + \frac{1}{2}I_{2y}\cos(\Delta\Phi_{(1)})\cos(\Delta\Phi_{(2)})\sin^2(2\pi J_{II}\tau) \times \exp\left(\frac{-2\tau}{T'_{2(1)}}+\frac{-2\tau}{T'_{2(2)}}\right) \tag{16}$$

$$I_{2x} \xrightarrow{\text{RDR, DQF, RDR}} \frac{1}{2}I_{2x}\cos^2(\Delta\Phi_{(2)})\sin^2(2\pi J_{II}\tau)\exp\left(\frac{-4\tau}{T'_{2(2)}}\right) + \frac{1}{2}I_{1y}\cos(\Delta\Phi_{(2)})\cos(\Delta\Phi_{(1)})\sin^2(2\pi J_{II}\tau) \times \exp\left(\frac{-2\tau}{T'_{2(2)}}+\frac{-2\tau}{T'_{2(1)}}\right) \tag{17}$$

The dipolar evolution time corresponds to that of one REDOR unit ($N_cT_r = 8nT_r$). The echo delay (τ) is an integer multiple of the rotor period ($\tau = 4nT_r + T_r$). The signal is given by the sum of Eqs. (16) and (17) because I_{1x} and I_{2x} are excited simultaneously. The full-echo signal intensity (S_0) for I_1 after the phase cycling of Table 1 is [14]

$$\begin{aligned} S_0 &= \frac{1}{2}\sin^2(2\pi J_{II}\tau)\left[\exp\left(\frac{-4\tau}{T'_{2(1)}}\right)+\exp\left(\frac{-2\tau}{T'_{2(1)}}+\frac{-2\tau}{T'_{2(2)}}\right)\right] \times \frac{1}{4\pi^2}\int_\beta\int_\alpha\int_\phi \mathrm{d}\phi\,\mathrm{d}\alpha\sin\beta\,\mathrm{d}\beta \\ &= \frac{1}{2}\sin^2(2\pi J_{II}\tau)\left[\exp\left(\frac{-4\tau}{T'_{2(1)}}\right)+\exp\left(\frac{-2\tau}{T'_{2(1)}}+\frac{-2\tau}{T'_{2(2)}}\right)\right] \times \frac{1}{2\pi}\int_{\beta_1}\int_{\alpha_1}\mathrm{d}\alpha_1\sin\beta_1\,\mathrm{d}\beta_1 \end{aligned} \tag{18}$$

The factor of 1/2 in Eq. (18) arises from the double-quantum selection, which involves taking the average of signal intensities for the first two phase entries of Table 1. The expression for the full-echo intensity is similar to that of conventional REDOR, but includes J_{II} and T'_2 modulations. The DQF–REDOR signal intensity (S) for I_1 under full dephasing (^{15}N π pulses during both τ–π–τ dipolar-evolution periods of Fig. 2) and phase cycling is

$$\begin{aligned} S &= \frac{1}{2}\sin^2(2\pi J_{II}\tau)\frac{1}{4\pi^2}\int_\beta\int_\alpha\int_\phi \mathrm{d}\phi\,\mathrm{d}\alpha\sin\beta\,\mathrm{d}\beta \times \left[\cos^2(\Delta\Phi_{(1)})\exp\left(\frac{-4\tau}{T'_{2(1)}}\right)+\cos(\Delta\Phi_{(1)})\cos(\Delta\Phi_{(2)}) \times \exp\left(\frac{-2\tau}{T'_{2(1)}}+\frac{-2\tau}{T'_{2(2)}}\right)\right] \\ &= \frac{1}{2}\sin^2(2\pi J_{II}\tau)\left[\exp\left(\frac{-4\tau}{T'_{2(1)}}\right)\frac{1}{2\pi}\int_{\beta_1}\int_{\alpha_1}\mathrm{d}\alpha_1\sin\beta_1\,\mathrm{d}\beta_1\cos^2(\Delta\Phi_{(1)}) + \exp\left(\frac{-2\tau}{T'_{2(1)}}+\frac{-2\tau}{T'_{2(2)}}\right)\frac{1}{4\pi^2} \times \int_\beta\int_\alpha\int_\phi \mathrm{d}\phi\,\mathrm{d}\alpha\sin\beta\,\mathrm{d}\beta\cos(\Delta\Phi_{(1)})\cos(\Delta\Phi_{(2)})\right] \end{aligned} \tag{19}$$

The first and the second terms in Eq. (19) correspond to the coherence pathways $I_{1x} \to I_{1x}$ and $I_{2x} \to I_{1y}$, respectively. The I–S dipolar coupling for the $I_{2x} \to I_{1y}$ term is $\omega_{D(2)}$ during the first τ–π–τ period, and $\omega_{D(1)}$ during the second τ–π–τ period; $\omega_{D(2)}$ and $\omega_{D(1)}$ are correlated by θ and r_{12} and REDOR dephasings dependent on these couplings cannot be calculated independently. Evaluation of the $I_{2x} \to I_{1y}$ term requires the correlated coordinate system of Fig. 4 (right) to retain the information about the orientation between S–I_1 and S–I_2.

The DQF–REDOR signal intensity (S) for I_1 under partial dephasing (^{15}N π pulses during the first τ–π–τ period only) is

$$\begin{aligned} S &= \frac{1}{2}\sin^2(2\pi J_{II}\tau)\frac{1}{4\pi^2}\int_\beta\int_\alpha\int_\phi \mathrm{d}\phi\,\mathrm{d}\alpha\sin\beta\,\mathrm{d}\beta\left[\cos(\Delta\Phi_{(1)})\exp\left(\frac{-4\tau}{T'_{2(1)}}\right) + \cos(\Delta\Phi_{(2)})\exp\left(\frac{-2\tau}{T'_{2(1)}}+\frac{-2\tau}{T'_{2(2)}}\right)\right] \\ &= \frac{1}{2}\sin^2(2\pi J_{II}\tau)\left[\exp\left(\frac{-4\tau}{T'_{2(1)}}\right)\frac{1}{2\pi}\int_{\beta_1}\int_{\alpha_1}\mathrm{d}\alpha_1\sin\beta_1\,\mathrm{d}\beta_1\cos(\Delta\Phi_{(1)}) + \exp\left(\frac{-2\tau}{T'_{2(1)}}+\frac{-2\tau}{T'_{2(2)}}\right)\frac{1}{2\pi}\int_{\beta_2}\int_{\alpha_2}\mathrm{d}\alpha_2\sin\beta_2\,\mathrm{d}\beta_2\cos(\Delta\Phi_{(2)})\right] \end{aligned} \tag{20}$$

The DQF–REDOR signal intensity (S) for I_1 under partial dephasing (^{15}N π pulses during the second τ–π–τ period) is

$$\begin{aligned} S &= \frac{1}{2}\sin^2(2\pi J_{II}\tau)\frac{1}{4\pi^2}\int_\beta\int_\alpha\int_\phi \mathrm{d}\phi\,\mathrm{d}\alpha\sin\beta\,\mathrm{d}\beta\left[\cos(\Delta\Phi_{(1)})\exp\left(\frac{-4\tau}{T'_{2(1)}}\right) + \cos(\Delta\Phi_{(1)})\exp\left(\frac{-2\tau}{T'_{2(1)}}+\frac{-2\tau}{T'_{2(2)}}\right)\right] \\ &= \frac{1}{2}\sin^2(2\pi J_{II}\tau)\left[\exp\left(\frac{-4\tau}{T'_{2(1)}}\right)+\exp\left(\frac{-2\tau}{T'_{2(1)}}+\frac{-2\tau}{T'_{2(2)}}\right)\right] \times \frac{1}{2\pi}\int_{\beta_1}\int_{\alpha_1}\mathrm{d}\alpha_1\sin\beta_1\,\mathrm{d}\beta_1\cos(\Delta\Phi_{(1)}) \end{aligned} \tag{21}$$

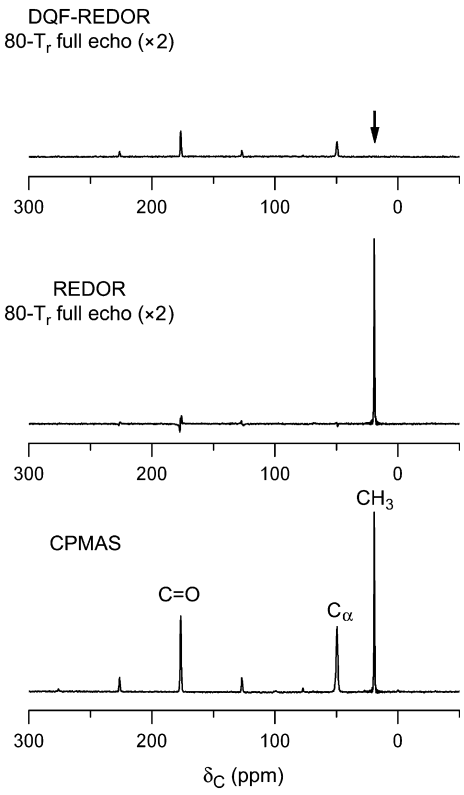

Fig. 5. 125-MHz magic-angle spinning ^{13}C NMR spectra of the mix of alanines of Fig. 1 obtained using a matched proton–carbon cross-polarization transfer (bottom), followed by 80 rotor cycles of evolution with a single ^{13}C refocusing π pulse (middle), or 80 rotor cycles of evolution with a $\tau = 20\text{-}T_r$ double-quantum filter (top). Four times as many scans were accumulated for the two echo spectra as for the CPMAS spectrum. The middle and bottom spectra have been scaled for equal methyl-carbon peak intensities. Magic-angle spinning was at 6250 Hz.

Both first and second partial dephasings can be evaluated using the independent coordinate system of Fig. 4 (left). The scaled DQF–REDOR difference for I_1 under partial dephasing during the second τ–π–τ period is $\Delta S/S_0 = (S_0 - S)/S_0$, where S_0 and S are given by Eqs. (18) and (21), respectively. Because the modulation pre-factors for S and S_0 are the same under partial dephasing during just the second τ–π–τ period, this $\Delta S/S_0$ ratio is identical to that for conventional REDOR [1]. Similar expressions can be written for the full-echo, DQF–REDOR, and scaled DQF–REDOR difference signal intensities for I_2.

3.3. Alanine spectra

The cross-polarization magic-angle spinning ^{13}C NMR spectrum of the mix of alanines shows the expected three isotropic peaks (and carbonyl-carbon sidebands) indicating approximately equal concentrations of the three ^{13}C labels (Fig. 5, bottom). After 80 rotor cycles (12.8 ms), the REDOR full-echo spectrum is reduced to just the methyl-carbon peak (Fig. 5, middle) because the two ^{13}C–^{13}C signals are largely dephased by the 54-Hz scalar J coupling [19]. Using the sequence of Fig. 2 on the other hand, the ^{13}C–^{13}C signals are strong and in phase (Fig. 5, top), and the single-^{13}C methyl-carbon signal is totally suppressed (arrow). The DQF–REDOR carbonyl-carbon peak is about 33% of that expected for a Hahn echo after 12.8 ms, based on comparison to the equal methyl-carbon peak heights (Fig. 5, middle and bottom), which have been scaled to account for homogeneous decay. We attribute two-thirds of the reduction to losses associated with the finite ^{13}C pulses of the double-quantum filter and the carbonyl-carbon T_2', and one-third to modulation by J_{CC} ($\sin^2 2\pi J\tau \approx 0.8$) and the α-carbon T_2'. Refocusing was reduced further by moving the REDOR pulses at the completion of rotor cycles from the ^{13}C channel (Fig. 2) to the ^{15}N channel. The DQF–REDOR α-carbon signal is reduced relative to the corresponding carbonyl-carbon signal because of the somewhat shorter echo-train lifetime for the α-carbon.

3.4. Alanine REDOR dephasing

If both τ–π–τ periods are used, the dephasing rates for the two carbons are similar but not identical and the maximum $\Delta S/S_0$ is less than 1 (Fig. 6). Both of these effects result from a dependence of the DQF $\Delta S/S_0$ on the products of dephasing terms involving J and the two I–S dipolar couplings but not their average (Eq. (19)).

If only the first of the τ–π–τ periods of Fig. 2 is used for dephasing, the observed DQF $\Delta S/S_0$ for the α- and carbonyl carbons are almost the same (Fig. 7). In this situation, the DQF $\Delta S/S_0$ depends on a T_2-weighted average I–S dipolar coupling (Eq. (20)). However, if only the second of the τ–π–τ periods of Fig. 2 is used for dephasing, the observed DQF $\Delta S/S_0$ for the α- and carbonyl-carbon are equal to those in a conventional REDOR experiment (text following Eq. (21)). Full dephasing occurs for the α-carbon in a little less than 2 ms, and for the carbonyl carbon in about 8 ms (Fig. 8).

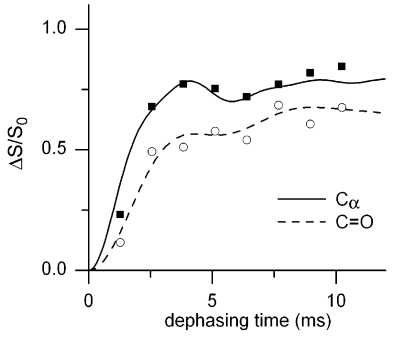

Fig. 6. $^{13}C\{^{15}N\}$ DQF–REDOR dephasing ($\Delta S/S_0$) for the mix of alanines of Fig. 3 using the pulse sequence of Fig. 2 with ^{15}N dephasing pulses during both τ–π–τ periods. The observed dephasing (symbols) is consistent with that calculated (solid and dotted lines) for the ^{13}C–^{13}C–^{15}N spin system (Eq. (20)), assuming a $^{13}C(=O)$–^{15}N distance of 1.49 Å, a $^{13}C_\alpha$–^{15}N distance of 2.47 Å, a $^{13}C_\alpha$–$^{13}C{=}O$ distance of 1.53 Å, and full-echo lifetimes for 10 ms of evolution of 4.18 ms (C_α, filled squares) and 5.93 ms (C=O, open circles).

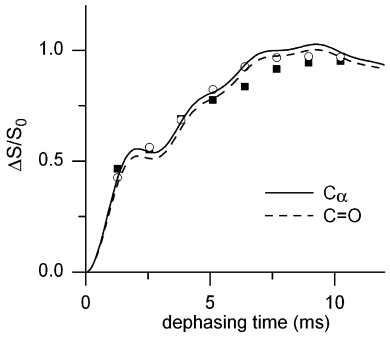

Fig. 7. $^{13}C\{^{15}N\}$ DQF–REDOR dephasing ($\Delta S/S_0$) for the mix of alanines of Fig. 1 using the pulse sequence of Fig. 2 with ^{15}N dephasing pulses during just the first τ–π–τ period. The observed dephasing (symbols) is consistent with that calculated (solid and dotted lines) for the ^{13}C–^{13}C–^{15}N spin system and the parameters of Fig. 6.

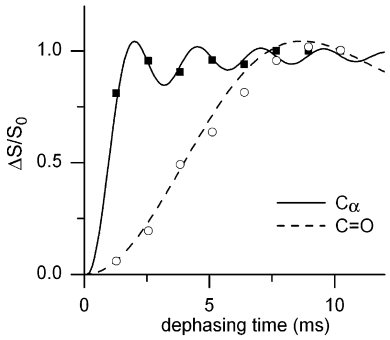

Fig. 8. $^{13}C\{^{15}N\}$ DQF–REDOR dephasing ($\Delta S/S_0$) for the mix of alanines of Fig. 1 using the pulse sequence of Fig. 2 but with ^{15}N dephasing pulses during only the second τ–π–τ period. The dephasing is identical to that of conventional REDOR. The observed dephasing (symbols) is consistent with that calculated (solid and dotted lines) for the ^{13}C–^{13}C–^{15}N spin system and the parameters of Fig. 6.

3.5. Application to glycine metabolism in soybean leaves

Recently, we used solid-state ^{13}C NMR measurements of intact soybean leaves labeled by $^{13}CO_2$ (at sub-ambient concentrations) [20] to show that excess glycine from the photorespiratory C_2 cycle (i.e., glycine not part of the production of glycerate in support of photosynthesis) is either fully decarboxylated or inserted as ^{13}C-labeled glycyl residues in proteins [21]. This ^{13}C incorporation in leaf protein, which was also uniformly ^{15}N labeled by $^{15}NH_4{}^{15}NO_3$, occurs as soon as 2 min after the start of $^{13}CO_2$ labeling. These measurements were based on differences between the spectra of labeled leaves and those of similar unlabeled leaves. A difference of this sort usually suffers from phase and amplitude distortions. Because the glycine from the C_2 cycle is 50% ^{13}C-enriched within 2 min of the start of labeling, and more than 95% within 4 min [20], we can use a DQF ^{13}C–^{13}C filter to follow glycine metabolism in a labeled leaf with no interference from the natural-abundance background. A separate experiment on an unlabeled leaf is not required and this makes up for most of the losses in the double-quantum filter. The DQF–REDOR strategy

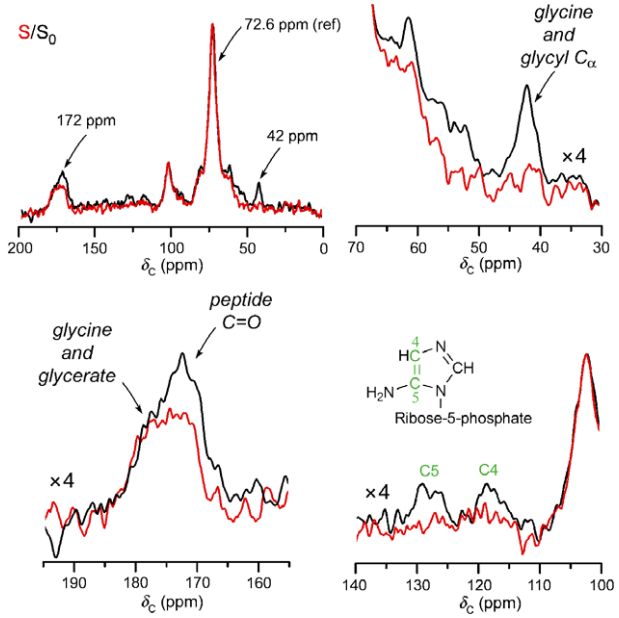

Fig. 9. 125-MHz $^{13}C\{^{15}N\}$ DQF–REDOR spectra of a lyophilized soybean leaf (150 mg) labeled for 6 min with 300-ppm $^{13}CO_2$. The full-echo spectrum is shown in black and the ^{15}N-dephased spectrum in red. The double-quantum filter was optimized (maximum full echo) for 56 rotor periods ($\tau = 4\ nT_r + 2T_r = 14\ T_r$, magic-angle spinning at 7143 Hz, $4\tau = 7.84$ ms). Dephasing was restricted to 12 rotor periods during the second τ–π–τ period. Both S and S_0 spectra resulted from the accumulation of 480,000 scans.

is illustrated in Fig. 9 where the appearance of ^{13}C–^{13}C pairs in glycine, glycerate, and glycyl residues in protein [21], as well as in glycyl insertions in aminoimidazole purine precursors, is made clear by the combination of characteristic chemical shifts and one-bond REDOR dephasing by ^{15}N. The double-quantum filter also passes ^{13}C–^{13}C coherences that arise from the triose components of sugars (73 and 105 ppm) produced by photosynthesis [20]. These sugar signals are not dephased by ^{15}N.

3.6. Conclusions

We have shown that DQF–REDOR, a combination of a ^{13}C–^{13}C homonuclear *J*-based double-quantum filter and $^{13}C\{^{15}N\}$ REDOR, results in selective observation of ^{13}C–^{13}C spin pairs in the presence of a large background signal from ^{13}C single spins. Internuclear distances between the ^{13}C–^{13}C spin pairs and an ^{15}N dephaser can be measured quantitatively without the complication of the unadjustable phase twist and dephasing caused by J_{CC} coupling. DQF–REDOR is suitable for analyses as complicated as the tracking of glycine metabolism in a *uniform*-^{15}N soybean leaf labeled by $^{13}CO_2$.

References

[1] T. Gullion, J. Schaefer, Detection of weak heteronuclear dipolar coupling by rotational-echo double-resonance NMR, Adv. Magn. Reson. 13 (1989) 58–83.

[2] C.M. Rienstra, Magic-angle spinning recoupling techniques for distance determinations among spin-1/2 nuclei in solid peptides and proteins, in: A. Ramomoorthy (Ed.), NMR Spectroscopy of Biological Solids, CRC Press, Boca Raton, 2006, pp. 2–29.
[3] A.K. Mehta, L. Cegelski, R.D. O'Connor, J. Schaefer, REDOR with a relative full-echo reference, J. Magn. Reson. 163 (2003) 182–187.
[4] S.M. Holl, G.R. Marshall, D.D. Beusen, K. Kociolek, A.S. Redlinski, M.T. Leplawy, R.A. McKay, S. Vega, J. Schaefer, Determination of an 8-Å interatomic distance in a helical peptide by solid-state NMR spectroscopy, J. Am. Chem. Soc. 114 (1992) 4830–4833.
[5] O. Toke, R.D. O'Connor, T.K. Weldeghiorghis, W.L. Maloy, R.W. Glaser, A.S. Ulrich, J. Schaefer, Structure of $(KIAGKIA)_3$ aggregates in phospholipid bilayers by solid-state NMR, Biophys. J. 87 (2004) 675–687.
[6] A.W. Hing, S. Vega, J. Schaefer, Measurement of heteronuclear dipolar coupling by transferred-echo double-resonance NMR, J. Magn. Reson. 103 (1993) 151–162.
[7] L. Cegelski, D. Steuber, A.K. Mehta, D.W. Kulp, P.H. Axelsen, J. Schaefer, Conformational and quantitative characterization of oritavancin–peptidoglycan complexes in whole cells of *Staphylococcus aureus* by *in vivo* ^{13}C and ^{15}N labeling, J. Mol. Biol. 357 (2006) 1253–1262.
[8] D.R. Studelska, L.M. McDowell, M. Adler, R.D. O'Connor, A.K. Mehta, W.J. Guilford, J.L. Dallas, D. Arnaiz, D.R. Light, J. Schaefer, Conformation of a bound inhibitor of blood coagulant factor Xa, Biochemistry 42 (2003) 7942–7949.
[9] K. Schmidt-Rohr, H.W. Spiess, Multidimensional Solid-State NMR and Polymers, Academic Press, San Diego, 1994, pp. 212–213.
[10] A.J. Shaka, R. Freeman, Simplification of NMR spectra by filtration through multiple-quantum coherence, J. Magn. Reson. 51 (1983) 169–173.
[11] A. Bax, R. Freeman, S.P. Kempsell, Natural abundance carbon-13-carbon-13 coupling observed via double-quantum coherence, J. Am. Chem. Soc. 102 (1980) 4849–4851.
[12] A. Lesage, M. Bardet, L. Emsley, Through-bond carbon–carbon connectivities in disordered solids by NMR, J. Am. Chem. Soc. 121 (1999) 10987–10993.
[13] R. Verel, J.D. van Beek, B.H. Meier, INADEQUATE-CR experiments in the solid state, J. Magn. Reson. 140 (1999) 300–303.
[14] L.J. Mueller, D.W. Elliott, G.M. Leskowitz, J. Struppe, R.A. Olsen, K.-C. Kim, C.A. Reed, Uniform-sign cross-peak double-quantum-filtered correlation spectroscopy, J. Magn. Reson. 168 (2004) 327–335.
[15] J. Schaefer, R.A. McKay, Multi-tuned single coil transmission line probe for nuclear magnetic resonance spectrometer, US Patent 5,861,748 (1999).
[16] D. Stueber, A.K. Mehta, Z. Chen, K.L. Wooley, J. Schaefer, Local order in polycarbonate glasses by $^{13}C\{^{19}F\}$ rotational-echo double-resonance NMR, J. Poly. Sci. Phys. (2006), doi:10.1002/polb.20931.
[17] T. Gullion, D.B. Baker, M.S. Conradi, New compensated Carr-Purcell sequences, J. Magn. Reson. 89 (1990) 479–484.
[18] A.E. Bennett, C.M. Rienstra, M. Auger, K.V. Lakshmi, R.G. Griffin, Heteronuclear decoupling in rotating solids, J. Chem. Phys. 103 (1995) 6951–6958.
[19] A.K. Mehta, J. Schaefer, Rotational-echo double resonance of uniformly labeled ^{13}C clusters, J. Magn. Reson. 163 (2003) 188–191.
[20] L. Cegelski, J. Schaefer, NMR determination of photorespiration in intact leaves using *in vivo* $^{13}CO_2$ labeling, J. Magn. Reson. 178 (2006) 1–10.
[21] L. Cegelski, J. Schaefer, Glycine metabolism in intact leaves by *in vivo* ^{13}C and ^{15}N labeling, J. Biol. Chem. 280 (2005) 39238–39245.